

# Effects of relevant parameters on the bandgaps of acoustic metamaterials with multi-resonators

Xiaoqin Zhou<sup>1</sup> · Jun Wang<sup>1</sup> · Rongqi Wang<sup>1</sup> · Jieqiong Lin<sup>2</sup>

Received: 5 December 2015 / Accepted: 7 March 2016 / Published online: 21 March 2016  
© Springer-Verlag Berlin Heidelberg 2016

**Abstract** Locally resonant acoustic metamaterials with multi-resonators are generally regarded as a fine trend for managing the bandgaps, the different effects of relevant structural parameters on the bandgaps, which will be numerically investigated in this paper. A two-step homogenization method is extended to achieve the effective mass of multi-resonators metamaterial in the lattice system. As comparison, the dispersive wave propagation in lattice system and continuum model is studied. Then, the different effects of relevant parameters on the center frequencies and bandwidth of bandgaps are perfectly revealed, and the steady-state responses in the continuum models with purposed relevant parameters are additionally clarified. The related results can well confirm that the bandgaps exist around the undamped natural frequencies of internal resonators, and also their bandwidth can be efficiently controlled with the ensured center frequencies. Moreover, the design of purposed multi-resonators acoustic metamaterial in vibration control is presented and discussed by an example.

## 1 Introduction

The acoustic metamaterials (AMs), which have attracted many significant attentions due to their distinctive properties recently, mainly focus on their negative dynamic

effective parameters, such as the negative bulk modulus and mass density that are hardly observed in the traditional natural materials [1]. In 2000, a seminal paper was published for conceptually realizing an AM involving the locally resonant structural units [2], which can exhibit the negative mass near the natural frequency of internal resonator. Fang et al. [3] reported a class of ultrasonic metamaterials with the subwavelength Helmholtz resonators that can possess negative dynamic modulus near the resonance frequency. The metamaterial simultaneously owning double negativity was achieved by the independent combination of structures consisting of the negative modulus and mass density unit [4]. Subsequently, various metamaterials with single or double negativity have been presented based on different mechanisms [5–7]. When the wavelength of elastic waves is long compared to the feature size of metamaterials, the homogenization theories can be employed because the metamaterials behave as effective homogeneous media [8] in this situation. The lattice models of metamaterials were constructed with concentrated masses and connected springs to investigate the effective parameters [9]. Currently, a two-step homogenization method (HM) was introduced to obtain the effective parameters of single-resonator metamaterials, which was more convenient for further analysis [10]. Meanwhile, many researchers have also devoted themselves to exploring various significant applications of the AMs, such as the vibration/noise isolation [11–13], cloak [14], waveguiding [15] and sensors applying in measuring liquid properties [16] or nondestructive testing [17].

For locally resonant AMs with single resonator, the frequency region of negative effective parameters is not enough for their practical applications generally [10]; therefore, the optimizing process for the bandgaps of these AMs is very necessary. For example, Lee et al. [18] and

✉ Xiaoqin Zhou  
xqzhou@jlu.edu.cn

<sup>1</sup> School of Mechanical Science and Engineering,  
Jilin University, Changchun 130022, China

<sup>2</sup> School of Electromechanical Engineering, Changchun  
University of Technology, Changchun 130012, China

Yang et al. [19] presented a type of thin membrane-type structures to construct broadband metamaterials, as well as Ding et al. [6] achieved the negative effective bulk modulus based on the split hollow sphere. Besides traditionally searching novel complex structures, the existing structures with multi-resonators are fine trends for managing the bandgaps. For instance, Huang and Sun [20] demonstrated that there are three bandgaps in mass-in-mass lattice systems with dual resonators that have been found to be available to optimize the negative effective mass density by Tan et al. [21]. In addition, Pai et al. [22] also demonstrated that two stop bands exist around the high-frequency side of the local resonance frequencies of two-mass absorber, respectively, on a metamaterial beam. Here, we present some extensive works from the previous works and clarify the different effects of structure parameters in continuum model.

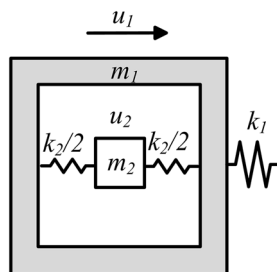
In this paper, a one-dimensional (1-D) lattice model of the AMs with multi-resonators will be fully considered, and the convenient two-step HM which can accurately match the dispersion relations will be expanded to acquire the effective parameters of AMs in Sect. 2. Then, the effects of relevant parameters on the center frequency and bandwidth of the bandgaps are analytically revealed in Sect. 3. In Sect. 4, the wave propagation in specific continuum models based on mimicking lattice systems [10] is analyzed by the finite element method (FEM), and an application example of the purposed multi-resonators AM in vibration control is presented and discussed.

## 2 Locally resonant acoustic metamaterials

### 2.1 Effective mass and bandgaps in lattice model with single resonator

The negativity effective mass in a lattice model of mass-in-mass unit was demonstrated by Huang et al. [9], the unit employed a 1-D monatomic lattice with a single internal resonator, as shown in Fig. 1. For the harmonic input  $F(t)$  and the response  $u_i(t)$ , the equation of motion for the unit is derived as Eq. (1).

**Fig. 1** Mass-in-mass lattice unit with single internal resonator



$$\begin{bmatrix} m_1 & 0 \\ 0 & m_2 \end{bmatrix} \begin{Bmatrix} \ddot{u}_1 \\ \ddot{u}_2 \end{Bmatrix} + \begin{bmatrix} k_2 & -k_2 \\ -k_2 & k_2 \end{bmatrix} \begin{Bmatrix} u_1 \\ u_2 \end{Bmatrix} = \begin{Bmatrix} F \\ 0 \end{Bmatrix} \quad (1)$$

Then, the effective mass  $m_{\text{eff}}$  is expressed by

$$m_{\text{eff}} = m_1 + \frac{m_2}{1 - \omega^2/\omega_n^2} \quad (2)$$

where  $\omega_n = \sqrt{k_2/m_2}$  is the natural frequency of internal resonator,  $\omega$  is the angular frequency. In the case of  $\theta = m_2/m_1 = 1$ , the negative effective mass  $m_{\text{eff}}/m_{\text{st}}$  becomes negative within the range of  $1 < \omega/\omega_n < \sqrt{1 + \theta}$ , as shown in Fig. 2a.

Taking the harmonic wave propagation into account, the dispersion equation of this mass-in-mass chain with single resonator can be derived by below:

$$m_1 m_2 \omega^4 - (m_1 + m_2) k_2 \omega^2 - k_1 (m_2 \omega^2 + k_2) \times (2 - e^{-iqL} - e^{iqL}) = 0 \quad (3)$$

where  $q$  denotes the wave number,  $L$  represents the length of each unit cell. There are two obvious bandgaps of the dispersion curves, namely  $0.7654 < \omega/\omega_n < 1.414$  and  $1.848 < \omega/\omega_n$ , as shown in Fig. 2b. The negative effective mass region is smaller than the first bandgap, for the reason that the negative effective mass  $m_{\text{eff}}$  of the mass-in-mass unit results from the inertia force of the internal lumped mass which is unrelated to spring  $k_1$ . The upper frequency of the first bandgap is equal to that of the negative effective mass; meanwhile, the starting frequency  $\omega = \omega_n$  of the negative effective mass is same with the center frequency of the first bandgap with the maximum attenuation coefficient. In other words, the center frequency of bandgaps mainly depends on the natural frequency of internal resonator, which is generally insensitive to other outer structure, while the bandwidth needs to be future investigated.

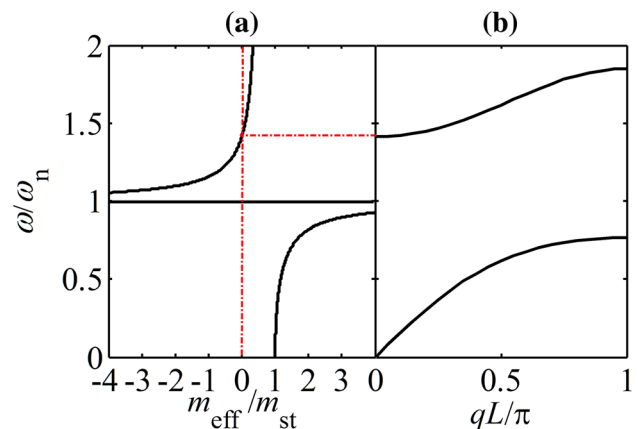


**Fig. 2** Comparison of the results,  $m_{\text{st}} = m_1 + m_2$ ,  $\theta = m_2/m_1$ ,  $\delta = k_2/k_1$  **a** effective mass obtained by Eq. (2) with  $\theta = 1$ , **b** dispersion curves by Eq. (3) with  $\theta = 1$ ,  $\delta = 2$

### 2.2 Acoustic metamaterials with multi-resonators

The multi-resonant lattice unit is a  $n$ -degree-of-freedom ( $n$ -DOF) system, as shown in Fig. 3a, where  $n = 3, 4, \dots$ , which consists of  $n - 1$  coupled lumped masses inside. The corresponding undamped equation of motion is expressed as Eq. (4).

$$\begin{aligned}
 & \begin{bmatrix} m_1 & 0 & 0 & \dots & 0 \\ 0 & m_2 & 0 & \dots & 0 \\ 0 & 0 & m_3 & \dots & 0 \\ \vdots & \vdots & \vdots & \ddots & \vdots \\ 0 & 0 & 0 & \dots & m_n \end{bmatrix} \begin{Bmatrix} \ddot{u}_1 \\ \ddot{u}_2 \\ \ddot{u}_3 \\ \vdots \\ \ddot{u}_n \end{Bmatrix} \\
 & + \begin{bmatrix} k_2 + k_{n+1} & -k_2 & 0 & \dots & -k_{n+1} \\ -k_2 & k_2 + k_3 & -k_3 & \dots & 0 \\ 0 & -k_3 & k_3 + k_4 & \dots & \vdots \\ \vdots & \vdots & \vdots & \ddots & -k_n \\ -k_{n+1} & 0 & \dots & -k_n & k_n + k_{n+1} \end{bmatrix} \begin{Bmatrix} u_1 \\ u_2 \\ u_3 \\ \vdots \\ u_n \end{Bmatrix} \\
 & = \begin{Bmatrix} F \\ 0 \\ 0 \\ \vdots \\ 0 \end{Bmatrix}
 \end{aligned} \tag{4}$$

For the harmonic input  $F(t)$  and the response  $u_i(t)$

$$F(t) \equiv F_0 e^{i\omega t}, \quad u_n \equiv U_n e^{i\omega t} \tag{5}$$

Then, Eq. (4) can be rewritten as follows:

$$(-\omega^2 [M] + [K]) \{U\} = \{F\} \tag{6}$$

where

$$\begin{aligned}
 [M] &= \begin{bmatrix} m_1 & 0 & 0 & \dots & 0 \\ 0 & m_2 & 0 & \dots & 0 \\ 0 & 0 & m_3 & \dots & 0 \\ \vdots & \vdots & \vdots & \ddots & \vdots \\ 0 & 0 & 0 & \dots & m_n \end{bmatrix}, \\
 [K] &= \begin{bmatrix} k_2 + k_{n+1} & -k_2 & 0 & \dots & -k_{n+1} \\ -k_2 & k_2 + k_3 & -k_3 & \dots & 0 \\ 0 & -k_3 & k_3 + k_4 & \dots & \vdots \\ \vdots & \vdots & \vdots & \ddots & -k_n \\ -k_{n+1} & 0 & \dots & -k_n & k_n + k_{n+1} \end{bmatrix}, \\
 \{F\} &= \begin{Bmatrix} F_0 \\ 0 \\ 0 \\ \vdots \\ 0 \end{Bmatrix}.
 \end{aligned}$$

Therefore, the frequency response function matrix  $[H]$  can be expressed as follows:

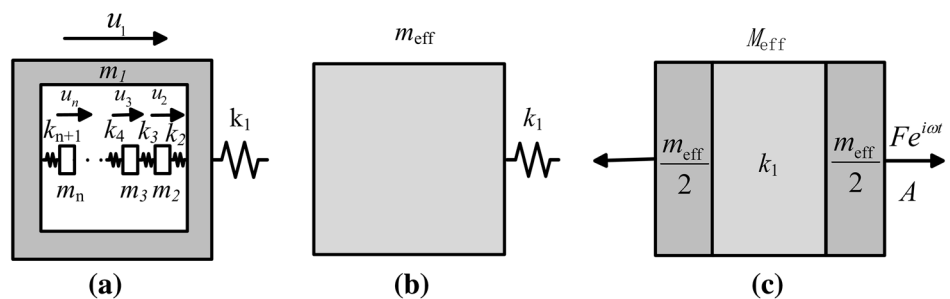
$$[H] = [-\omega^2 [M] + [K]]^{-1} \tag{7}$$

For  $m_{\text{eff}} = \frac{F(t)}{\ddot{u}_{\text{eff}}} = \frac{F_0}{-\omega^2 U_1}$ , the effective mass in the first-step homogenization, as shown in Fig. 3b, can be obtained as follows:

$$m_{\text{eff}} = \frac{1}{-\omega^2 H(1, 1)} \tag{8}$$

For the edges of bandgaps in lattice model with single resonator, a two-step HM has been introduced by Liu et al. [10]. In the first-step homogenization, the effective mass  $m_{\text{eff}}$  of the mass-in-mass unit above is obtained. Next in the

**Fig. 3** a Multi-resonant lattice unit, b effective mass in the first-step homogenization, c effective mass in the second-step homogenization



second-step HM, the infinite lattice system of the effective mass  $m_{\text{eff}}$  connected by the spring  $k_1$  can be regarded as an equivalent homogeneous material with mass  $M_{\text{eff}}$  and constant elastic coefficient  $k_1$ , as shown in Fig. 3c. On the other hand, the equivalent homogeneous material can be treated with the effective mass  $m_{\text{eff}}$  and effective elastic coefficient  $k_{\text{eff}}$ , where  $k_{\text{eff}} = F/2A$  would be obtained by the kinematic equation of the unit cell  $-m_{\text{eff}}\omega^2 A/2 = F - 2k_1 A$ , where  $A$  is the vibration amplitude of mass. By setting  $M_{\text{eff}}/k_1 = m_{\text{eff}}/k_{\text{eff}}$ , the effective mass  $M_{\text{eff}}$  in the second-step HM is derived to be

$$M_{\text{eff}} = \frac{m_{\text{eff}}k_1}{k_1 - m_{\text{eff}}\omega^2/4} \tag{9}$$

For example, the effective mass of lattice model with two and three resonators in the two-step HM is illustrated

resonators are set directly here:  $\theta_1 = m_2/m_3 = 2$ ,  $\delta_2 = k_2/k_4 = 1$  and  $\theta_2 = m_2/m_4 = 4$ ,  $\delta_3 = k_2/k_5 = 1$ . There are two negative ranges of the effective mass  $m_{\text{eff}}$  and three negative ranges of the effective mass  $M_{\text{eff}}$  with two resonators. When the third internal resonator is added, the effective mass  $m_{\text{eff}}$  becomes negative in three ranges and the effective mass  $M_{\text{eff}}$  has four negative ranges. It is obvious that the added coupled resonators gain more stop bands and broader bandwidth beyond the cutoff frequency of the lattice chain, which would be useful in designing AMs structures like bars or beams. However, the more resonators in the confined space of single unit will demand more complex manufacturing techniques.

For comparison, the dispersion equation of this multi-resonant lattice model for harmonic wave propagation is achieved by the Bloch–Floquet theory [23] as follows:

$$\begin{vmatrix} k_2 + k_{n+1} + 2k_1(1 - \cos(qL)) - m_1\omega^2 & -k_2 & 0 & \dots & -k_{n+1} \\ -k_2 & k_2 + k_3 - m_2\omega^2 & -k_3 & \dots & 0 \\ 0 & -k_3 & k_3 + k_4 - m_3\omega^2 & \dots & \vdots \\ \vdots & \vdots & \vdots & \ddots & -k_n \\ -k_{n+1} & 0 & \dots & -k_n & k_n + k_{n+1} - m_n\omega^2 \end{vmatrix} = 0 \tag{10}$$

in Fig. 4a, b, respectively, which correspond to  $n = 3$  and  $n = 4$ . In contrast, the same referred frequency  $\omega_0 = \sqrt{k_2/m_2}$  is adopted here, which is also the nature frequency of single internal resonator in Sect. 2.1. Then, the relevant parameters for the added second and third

There are three stop bands for double resonators and four stop bands for three resonators as shown in Fig. 4c. The frequency range of negative effective  $m_{\text{eff}}$  is included in the stop bands, while the negative effective mass  $M_{\text{eff}}$  can agree well with the bandgaps.

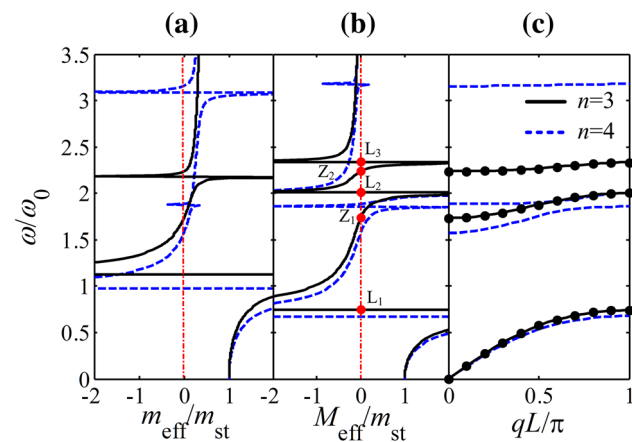


**Fig. 4** Comparison of the results, here  $m_{\text{st}} = m_1 + m_2 + \dots + m_n$  **a** effective mass  $m_{\text{eff}}$  in the first-step HM; **b** effective mass  $M_{\text{eff}}$  in the second-step HM; **c** the dispersion curves. The *solid* and *dashed* lines represent two and three resonators, respectively. The *points* describe the dispersion curves of the unit cell of continuum model by FEM

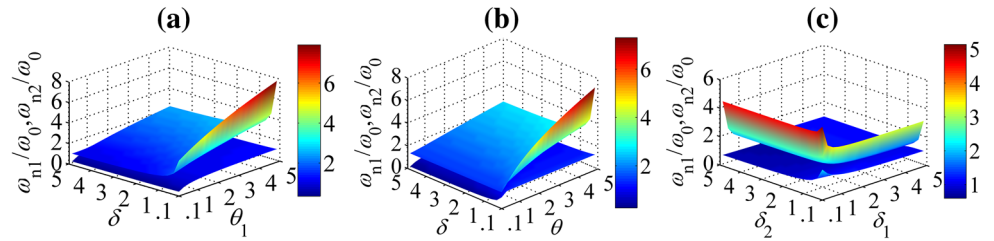
### 3 Relevant parameters on bandgaps of dual-resonator acoustic metamaterials

#### 3.1 Relevant parameters on the center frequencies of bandgaps

The center frequencies and bandwidth of bandgaps are the primary considerations on designing AMs. The effects of relevant parameters on the center frequencies of dual-resonator AMs are analyzed here. Under the parameters mentioned in the last chapter, Eq. (8) becomes

$$\begin{aligned} m_{\text{eff}}/m_{\text{st}} &= \frac{(9\theta + 6)\omega_0^4 - (2\theta + 6)\omega^2\omega_0^2 + \omega^4}{(1 + 1.5\theta)(\omega^2 - \omega_{n1}^2)(\omega^2 - \omega_{n2}^2)} \\ \omega_{n1}^2, \omega_{n2}^2 &= \frac{1}{2} \left[ \Omega \mp \sqrt{\Omega^2 - 4\theta_1[(1 + 1/\delta_1)(1/\delta_1 + 1/\delta_2) - 1/\delta_1^2]} \right] \\ \omega_0^2 &= 3 \mp \sqrt{3}\omega_0^2 \end{aligned} \tag{11}$$

**Fig. 5** Values of  $\omega_{n1}$ ,  $\omega_{n2}$ , namely the center frequencies of the former two bandgaps, **a** versus  $\theta_1$  and  $\delta_1$  with  $\delta_2 = 1$ , **b** versus  $\theta_1$  and  $\delta_2$  with  $\delta_1 = 1$ , **c** versus  $\delta_1$  and  $\delta_2$  with  $\theta_1 = 1$



where  $\Omega = 1 + 1/\delta_1 + \theta_1/\delta_1 + \theta_1/\delta_2$ . Here,  $\omega_{n1}$  and  $\omega_{n2}$  are the two undamped natural frequencies of internal resonators, which correspond to the two locations of asymptotes as the effective mass  $m_{eff}$  tends to infinity and the center frequencies of the first two bandgaps, respectively. The effects of relevant parameters  $\theta_1$ ,  $\delta_1$  and  $\delta_2$  on the value of  $\omega_{n1}$ ,  $\omega_{n2}$  are plotted in Fig. 5.  $\omega_{n1}$  is relatively smooth under the change of  $\theta_1$ ,  $\delta_1$  and  $\delta_2$ , while  $\omega_{n2}$  become extremely high when the value of  $\delta_1 \ll 1$  (Fig. 5a) or  $\delta_2 \ll 1$  (Fig. 5b). When both  $\delta_1$  and  $\delta_2$  tend to 0, the corresponding center frequencies of two bandgaps are increased simultaneously (Fig. 5c). As achieving low-frequency bandgaps is a meaningful topic of AMs, a lower value of  $\theta_1$ ,  $\delta_1 > 1$  and  $\delta_2 > 1$  is proposed. But it is unable to achieve multi-bandgaps fully below the bandgap of the single-resonator AMs due to the value of  $\omega_{n2}$  is always greater than  $\omega_0$ . Another interesting result is the case of  $\omega_{n1} = \omega_0$  (e.g.,  $\theta_1 = 1$ ,  $\delta_1 = 5$  and  $\delta_2 = 1$ ), where the multi-resonators AMs gain an extra stop band on the basis of the single-resonator AMs approximately.

### 3.2 Relevant parameters on the boundary frequencies of bandgaps

As shown in Fig. 4b, c, the points  $L_1$ – $L_3$ ,  $Z_1$ ,  $Z_2$  can agree well with the boundary frequencies of the three bandgaps in the dual-resonator model, where  $L_1$ – $L_3$  are the locations of the asymptotes as the effective mass  $M_{eff}$  tends to infinity and  $Z_1$ ,  $Z_2$  are the zero points of the effective mass  $M_{eff}$ . The first bandgap locates between  $L_1$  and  $Z_1$ , the second bandgap lies within the  $L_2$  and  $Z_2$ ; meanwhile, the third bandgap is the region exceeding  $L_3$ . When the central

frequencies of bandgaps have been determined by the certain values of  $\theta_1$ ,  $\delta_1$  and  $\delta_2$ , the values of five points are still affected by the mass ratio  $\theta$  and stiffness ratio  $\delta$ . For the first bandgap, the increasing  $\theta$  will result in a slightly wider bandwidth as illustrated in Fig. 6a. The bandwidth of the second pass band reaches a maximum value around  $\theta = 1$ , and the second stop band reaches the minimum value oppositely. Meanwhile, the third pass band is enlarged with the increase of  $\theta$  monotonically. It is noteworthy that the widths of both the second and third pass band are almost decreased to zero if the value of  $\theta$  is near zero, which is similar to the monatomic chains.

Figure 6b shows that the two zero points  $Z_1$  and  $Z_2$  are invariable with the value of  $\sqrt{(\theta + 3) \mp \sqrt{\theta^2 - 3\theta + 3}}$ , and both the first and second bandgap are broadened relatively with a higher value of  $\delta$ . If  $\delta$  is approach to zero just like the metamaterial beam [22], the third bandgap will begin at an extremely high frequency.

## 4 Continuum model and applications

### 4.1 Continuum model of multi-resonators acoustic metamaterials

Various continuum models have been put forward with the single negative mass density in last decade [4, 6, 7]; one of these models was presented by Sun et al. [10] based on the mimicking lattice systems, which can agree well with the theoretical result in lattice model. The similar continuum model with dual resonators is illustrated in Fig. 7.

**Fig. 6** Values of the points  $L_1$ – $L_3$ ,  $Z_1$  and  $Z_2$ , namely the edges of bandgaps **a** versus  $\theta = m_2/m_1$ , with  $\delta = k_2/k_1 = 1$ , **b** versus  $\delta$ , with  $\theta = 1$

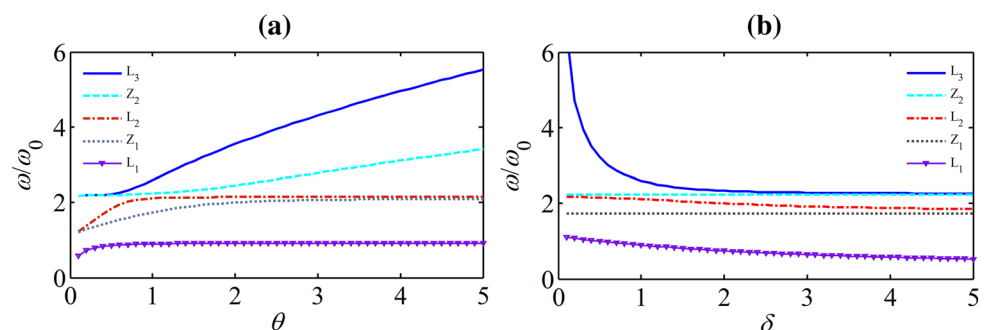


**Fig. 7** Continuum model of multi-resonant AM by mimicking lattice systems

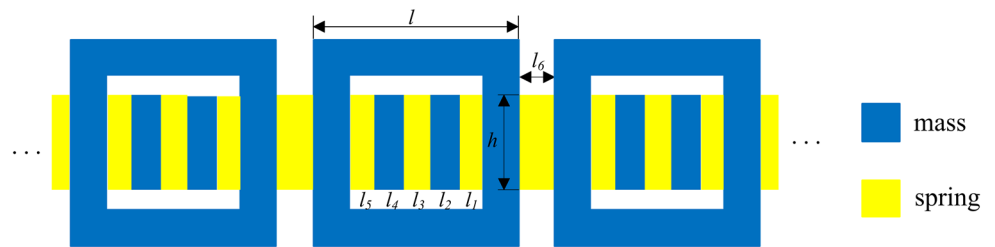


**Table 1** Dimensions of the continuum samples for proposed relevant parameters

Sample	Relevant parameters					Corresponding dimensions (mm)							
	$\theta$	$\delta$	$\theta_1$	$\delta_1$	$\delta_2$	$l$	$l_1$	$l_2$	$l_3$	$l_4$	$l_5$	$l_6$	$h$
S1	1	2	2	1	1	55.36	10	13.5	10	6.750	10	20	40
S2	1	2	<b>4</b>	1	1	55.36	10	13.5	10	<b>3.375</b>	10	20	40
S3	1	2	2	<b>0.25</b>	1	55.36	10	13.5	<b>2.5</b>	6.750	10	20	40
S4	1	2	2	1	<b>0.25</b>	55.36	10	13.5	10	6.750	<b>2.5</b>	20	40
S5	<b>0.25</b>	2	2	1	1	<b>68.45</b>	10	13.5	10	6.750	10	20	40
S6	<b>4</b>	2	2	1	1	<b>51.58</b>	10	13.5	10	6.750	10	20	40
S7	1	<b>0.25</b>	2	1	1	55.36	10	13.5	10	6.750	10	<b>2.5</b>	40

The differences between S1 and the rest samples appear in bold

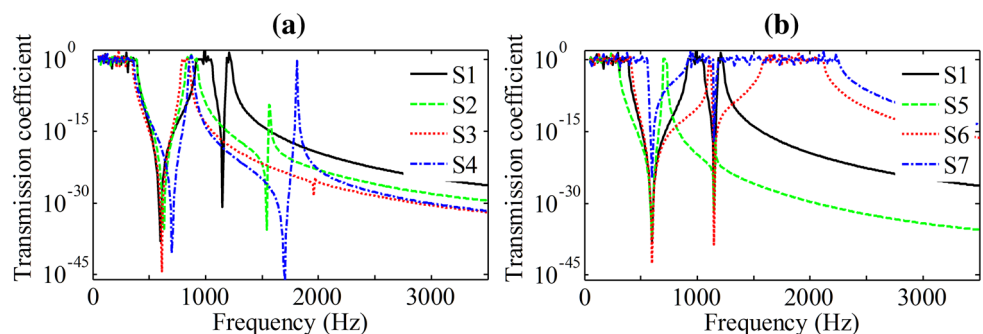
In this paper, the steel (density  $\rho = 7850 \text{ kg/m}^3$ , Young's modulus  $E = 210 \text{ GPa}$  and Poisson's ratio  $\mu = 0.29$ ) and the foam (density  $\rho = 115 \text{ kg/m}^3$ , Young's modulus  $E = 8 \text{ MPa}$  and Poisson's ratio  $\mu = 0.33$ ) [24] are selected to be the 'mass' and 'spring' materials, respectively. The purposed relevant parameters of the continuum models and the corresponding structure dimensions are listed in Table 1. The same referred frequency  $\omega_0 = \sqrt{k_2/m_2} = 3336.6 \text{ rad/s}$  is adopted here, which means the dimensions  $l_1$  and  $l_2$  are stable. The parameters of S1 are the same as the lattice model above, while the rest examples have only one relevant parameter different from the S1.

The wave propagation in these continuum models is investigated by FEM. The dispersion properties of the unit cell in S1 are analyzed by means of the Bloch–Floquet periodic boundary conditions. The first three dispersion curves of the unit cell are shown in Fig. 4c as the wave

vector varies along the contour of the first Brillouin zone, which has well agreement with dispersion equation Eq. (10). For the steady-state response, a one-dimensional 30 unit cell chain is employed, and a time harmonic displacement is then set as import boundary condition at the left end; meanwhile, the right end is set free. The transmission coefficient is defined as the ratio of the output displacements at the chosen locations to the import displacement. The transmission coefficients of the 15th unit of all the samples are shown in Fig. 8, respectively.

According to the two-step HM, three forbidden bands of the lattice model are calculated to be (398, 910 Hz), (1068, 1185 Hz) and (1240 Hz,  $+\infty$ ), as shown in Fig. 4, and the center frequencies of the first two bandgaps are 597 and 1155 Hz. From the transmission coefficients of S1 in Fig. 8, the edges of bandgaps are around 360, 920, 1050, 1190, 1220 Hz, and the center frequencies of the first two bandgaps are about 600 and 1150 Hz, which can well

**Fig. 8** Transmission coefficients of the samples in Table 1. **a** S1, S2, S3, S4 with varying  $\theta_1, \delta_1, \delta_2$ ; **b** S1, S5, S6, S7 with varying  $\theta, \delta$



coincide with the above predictions. The variable  $\delta_1$ ,  $\delta_2$  or  $\theta_1$  significantly affects the central frequencies of the first and second bandgaps, as shown in Fig. 8a, and the separate of the two central frequencies can broaden the second bandgap, but these variations have slight influence on the start frequency of the first bandgap. We can observe that two center frequencies of the first two bandgaps are independent of the variable  $\theta$  and  $\delta$  in Fig. 8b. A narrower bandwidth of the second pass band can be generated when  $\theta < 1$  or  $\theta > 1$ , but third pass band is broadened concurrently when  $\theta > 1$ . If the value of  $\delta$  is increased or  $\theta$  is approaching to zero, the start frequency of the first bandgap will be reduced.

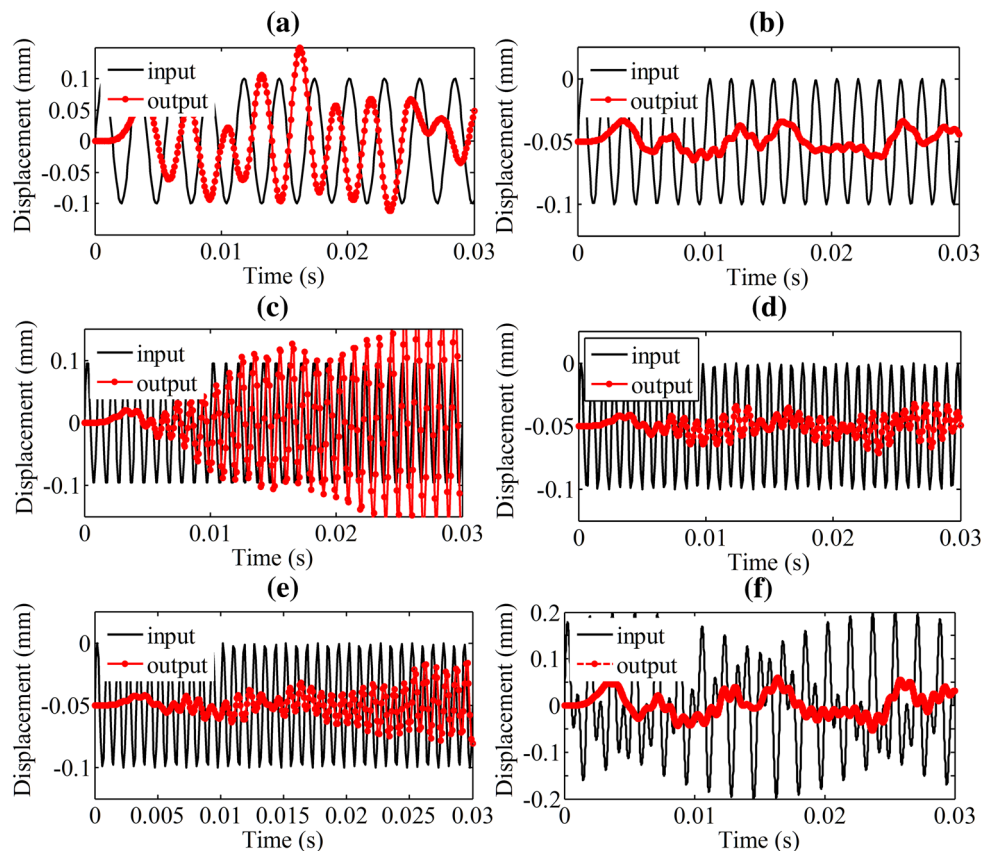
## 4.2 An application example

A natural practical application of these AMs is typical vibration control for the existence of bandgaps. Achieving suitable bandgaps which contain the frequency range of pernicious vibration or noise by adopting appropriate parameters is a basic demand. Obviously, the value of  $\omega_0 \approx \sqrt{E_k/\rho_m l_1 l_2}$  mainly depends on the density  $\rho_m$  of ‘mass’ material and Young’s modulus  $E_k$  of ‘spring’ material under confined space, the center frequencies of bandgaps would be firstly adjusted by  $\theta_1$ ,  $\delta_1$  and  $\delta_2$ ; then,

the bandwidth would be determined by  $\theta$  and  $\delta$ . For the moment, achieving low frequency or broad bandgaps for vibration control is a meaningful topic. A lower start frequency of the first bandgap can be obtained by a value of  $\theta$  near zero or a larger  $\delta$ , while the separate of  $\omega_{n1}$ ,  $\omega_{n2}$  or suitable values of  $\theta$  or  $\delta$  have significant influence on the bandwidth of both pass bands and forbidden bands.

The performances of the AM in vibration control are further studied here. An AM chain consisting of 5 unit cells of S1 is simulated by FEM. An input vibration displacement of  $U(0, t) = 0.1 (\sin 2\pi ft)$  is generated at one end of the model (1st unit cell) along the chain. At the opposite end (5th unit cell), the vibration output responses at different frequencies are achieved, as shown in Fig. 9. The metamaterial has tiny influence on the vibration transmission in the pass bands at  $f = 360$  Hz (Fig. 9a),  $f = 1000$  Hz (Fig. 9c),  $f = 1200$  Hz (Fig. 9e), and the output displacement become erratically due to the reflection of the vibration waves. While for the frequencies in the forbidden bands at  $f = 600$  Hz (Fig. 9b) and  $f = 1150$  Hz (Fig. 9d), the vibration waves will greatly decay as expected. Moreover, the vibration control with the multi-frequency excitation  $U(0, t) = 0.1(\sin 2\pi f_1 t + \sin 2\pi f_2 t)$  is also studied here, where  $f_1 = 600$  Hz,  $f_2 = 1150$  Hz. As shown in Fig. 9f, the structure is able to effectively

**Fig. 9** Displacement response with vibration input excitation at difference frequencies. **a** 360 Hz, **b** 600 Hz, **c** 1000 Hz, **d** 1150 Hz, **e** 1200 Hz, **f** 600 + 1150 Hz



attenuate the multi-frequency vibration wave. Further development of this model will have wider applications when these AMs are employed in the creation of vibration-less machining environment, as well as in the seismology: protecting buildings against earthquakes.

## 5 Conclusions

This paper reveals the effects of relevant parameters on the center frequencies and edges of bandgaps in multi-resonators AMs, and the results indicate the purposed meta-material can provide a possibility for managing the bandgaps instead of traditionally searching new complex structures or extreme component materials by tweaking the relevant parameters in the model. The two-step HM has been extended to obtain the effective mass of multi-resonators AM in lattice, which is confirmed available for multi-resonators AMs. Then, the dual-resonator continuum models based on the mimicking lattice systems with several special dimensions have been analyzed by the FEM, and the obtained results are in well agreement with the theoretical predictions, which can also demonstrate the validity of conclusions about the effects of the relevant parameters on bandgaps. Finally, the purposed multi-resonator AM has been verified to be feasible in vibration control under both the single-frequency and multi-frequency excitation with only five units. The present studies have further benefit for the design and applications of AMs.

**Acknowledgments** The authors are grateful to the financial support from the National Natural Science Foundation of China (NSFC) (51375060).

## References

1. M.I. Hussein, M.J. Leamy, M. Ruzzene, *Appl. Mech. Rev.* **66**(4), 040802 (2014)

2. Z. Liu, X. Zhang, Y. Mao, Y. Zhu, Z. Yang, C. Chan, P. Sheng, *Science* **289**(5485), 1734–1736 (2000)
3. N. Fang, D. Xi, J. Xu, M. Ambati, W. Srituravanich, C. Sun, X. Zhang, *Nat. Mater.* **5**(6), 452–456 (2006)
4. Y.Q. Ding, Z.Y. Liu, C.Y. Qiu, J. Shi, *Phys. Rev. Lett.* **99**(9), 093094 (2007)
5. Y. Wu, Y. Lai, Z.Q. Zhang, *Phys. Rev. Lett.* **107**(10), 105506 (2011)
6. C.L. Ding, L. M. Hao, X.P. Zhao, *J. Appl. Phys.* **108**(7), 074911 (2010)
7. S. Zhai, H. Chen, C. Ding, X. Zhao, *J. Phys. D Appl. Phys.* **46**(47), 475105 (2013)
8. D. Torrent, A. Håkansson, F. Cervera, J. Sánchez-Dehesa, *Phys. Rev. Lett.* **96**(20), 204302 (2006)
9. H.H. Huang, C.T. Sun, G.L. Huang, *Int. J. Eng. Sci.* **47**(4), 610–617 (2009)
10. Y. Liu, X. Su, C.T. Sun, *J. Mech. Phys. Solids* **74**, 158–174 (2015)
11. A. Climente, D. Torrent, J. Sánchez-Dehesa, *Appl. Phys. Lett.* **100**(14), 144103 (2012)
12. R.Q. Li, X.F. Zhu, B. Liang, Y. Li, X.Y. Zou, J.C. Cheng, *Appl. Phys. Lett.* **99**(19), 193507 (2011)
13. H.W. Sun, X.W. Du, P.F. Pai, *J. Intell. Mater. Syst. Struct.* **21**(11), 1085–1101 (2010)
14. S. Zhang, C. Xia, N. Fang, *Phys. Rev. Lett.* **106**(2), 024301 (2011)
15. A. Khelif, B. Djafari-Rouhani, J. Vasseur, P. Deymier, *Phys. Rev. B* **68**(2), 024302 (2003)
16. R. Lucklum, M. Ke, M. Zubtsov, *Sens. Actuators B: Chem.* **171**, 271–277 (2012)
17. M. Ruzzene, F. Scarpa, F. Soranna, *Smart Mater. Struct.* **12**(3), 363 (2003)
18. S.H. Lee, C.M. Park, Y.M. Seo, Z.G. Wang, C.K. Kim, *Phys. Rev. Lett.* **104**(5), 054301 (2010)
19. M. Yang, G. Ma, Z. Yang, P. Sheng, *Phys. Rev. Lett.* **110**(13), 134301 (2013)
20. G.L. Huang, C.T. Sun, *J. Vib. Acoust. Trans. ASME* **132**(3), 031003 (2010)
21. K.T. Tan, H.H. Huang, C.T. Sun, *Appl. Phys. Lett.* **101**(24), 241902 (2012)
22. P.F. Pai, H. Peng, S.Y. Jiang, *Int. J. Mech. Sci.* **79**, 195–205 (2014)
23. L. Brillouin, *J. Manuf. Sci. Eng.* **93**(3), 65 (1946)
24. Y. Lai, Y. Wu, P. Sheng, Z.-Q. Zhang, *Nat. Mater.* **10**(8), 620–624 (2011)